THE JOURNAL OF BIOLOGICAL CHEMISTRY
Vol. 280, No. 17, Issue of April 29, pp. 16601–16609, 2005
© 2005 by The American Society for Biochemistry and Molecular Biology, Inc.
Printed in U.S.A.

Catechol Oxidase-like Oxidation Chemistry of the 1–20 and 1–16 Fragments of Alzheimer's Disease-related β-Amyloid Peptide

THEIR STRUCTURE-ACTIVITY CORRELATION AND THE FATE OF HYDROGEN PEROXIDE*

Received for publication, October 12, 2004, and in revised form, February 3, 2005
Published, JBC Papers in Press, February 7, 2005, DOI 10.1074/jbc.M411533200

Giordano F. Z. da Silva, William M. Tay, and Li-June Ming‡

From the Department of Chemistry and Institute for Biomolecular Science, University of South Florida, Tampa, Florida 33620-5250

The Cu^{2+} complexes of the 1–16 and the 1–20 fragments of the Alzheimer's disease-related β-amyloid peptide (CuAβ) show significant oxidative activities toward a catechol-like substrate trihydroxylbenzene and plasmid DNA cleavage. The latter reflects possible oxidative stress to biological macromolecules, yielding supporting data to the pathological role of these soluble Aβ fragments. The former exhibits enzyme-like kinetics and is dependent on $[H_2O_2]$, exhibiting k_{cat} of 0.066 s^{-1} (6000-fold higher than the reaction without CuAβ) and k_{cat}/K_m of 37.2 $M^{-1}s^{-1}$ under saturating $[H_2O_2]$ of ~0.24%. This kinetic profile is consistent with metal-centered redox chemistry for the action of CuAβ. A mechanism is proposed by the use of the catalytic cycle of dinuclear catechol oxidase as a working model. Trihydroxylbenzene is also oxidized by CuAβ aerobically without H_2O_2, affording rate constants of 6.50×10^{-3} s^{-1} and 3.25 $M^{-1}s^{-1}$. This activity is also consistent with catechol oxidase action in the absence of H_2O_2, wherein the substrate binds and reduces the Cu^{2+} center first, followed by O_2 binding to afford the μ-η^2:η^2-peroxo intermediate, which oxidizes a second substrate to complete the catalytic cycle. A tetragonally distorted octahedral metal coordination sphere with three coordinated His side chains and some specific H-bonding interactions is concluded from the electronic spectrum of CuAβ, hyperfine-shifted ^1H NMR spectrum of CoAβ, and molecular mechanics calculations. The results presented here are expected to add further insight into the chemistry of metallo-Aβ, which may assist better understanding of the neuropathology of Alzheimer's disease.

Abnormal metal-ion homeostasis has been closely associated with several neurodegenerative diseases, including Parkinson's, amyotrophic lateral sclerosis, Creutzfeldt-Jakob disease (*i.e.* human "mad cow" or prion disease), and Alzheimer's disease (AD)[1] (1–4). Because high cytoplasmic concentrations of free metal ions are toxic and potentially lethal, intricate physiological pathways have evolved to transport and distribute metal ions to their targets, which include enzymes and proteins (5). With aging, physiological processes responsible for accurate delivery of metal ions break down and "leakage" of free metal ions can cause toxic effects to cells (6, 7). Divalent ions of redox-active transition metals have often been associated with oxidative stress and closely involved in the chemistry of reactive oxygen species (ROS), including hydrogen peroxide as well as superoxide and hydroxyl radicals (8). Because increase in intracellular concentrations of metal ions is closely related to the effects of aging, oxidative stress, and AD, there is considerable interest in investigating the connection between malfunction of regulatory processes such as metal transport and the presence of ROS with the pathology of AD.

The chemistry of redox-active metal complexes of β-amyloid peptide (Aβ) has been an area of intense focus in the study of AD. The aggregation of Aβ within the neocortex is closely related to the pathology of AD and has been shown to be induced by metal binding (9, 10). The Aβ peptides are generated by the cleavage of the ubiquitous amyloid precursor protein by α, β, and γ secretases (11). Aβ in the form of insoluble plaques contains up to millimolar amounts of Zn^{2+}, Cu^{2+}, and Fe^{3+} in the neocortical region of the brain (8); however, the cause/effect connection of the metallo-Aβ plaques with AD is still under debate (12). The metal coordination environment of the 1–40 and 1–42 peptides has been previously studied and their pH-dependent aggregation reported (10, 13). The results showed that the metal binding seemed to be non-stoichiometric with ~3.5 metal ions per pair of aggregated peptides and a cooperative binding pattern as the amount of aggregates increases (8). Because $A\beta_{1-42}$ and $A\beta_{1-40}$ have been shown to bind Zn^{2+}, Fe^{3+}, and Cu^{2+} with extremely low apparent dissociation constants by means of quantitative determination of the metal-complex precipitates (8), understanding of the metal-binding domain and its structure may shed light on the chemistry related to the neuropathology of AD.

Although the coagulation of the peptide plaques leaves little doubt that interaction with cytoplasmic molecules is unlikely, smaller fragments of the amyloid peptide are soluble and Aβ fibrils extend across membranes, exposing them to the cytoplasm. Recently, insulin-degrading enzyme has been shown to digest the longer Aβ peptides (40–42 amino acids) into smaller soluble fragments (14). Moreover, the cleavage of amyloid pre-

* This work on metallopeptides structure and activity was supported by the Research and Creative Award of the University of South Florida and the Petroleum Research Fund administrated by the American Chemical Society (Grant PRF AC 40851-AC3). The costs of publication of this article were defrayed in part by the payment of page charges. This article must therefore be hereby marked "*advertisement*" in accordance with 18 U.S.C. Section 1734 solely to indicate this fact.

L.-J. M. dedicates this article to his mother and to Dr. Shwu-Yeng Lin, who with great patience and kindness have been caring for their beloved better halves through some very difficult times of "losing mind." G. F. Z. S. dedicates this article to Ayres Baptista Mello and family, whose struggle with Alzheimer's disease has fueled the author's desire in gaining a better understanding of the mechanisms of this disease at the molecular level.

‡ To whom correspondence should be addressed: Dept. of Chemistry and Institute for Biomolecular Science, University of South Florida, 4202 E. Fowler Ave., SCA400, Tampa, FL 33620-5250. Tel.: 813-974-2220; Fax: 813-974-3203; E-mail: ming@shell.cas.usf.edu.

[1] The abbreviations used are: AD, Alzheimer's disease; Aβ, β-amyloid peptide; ds, double-stranded; ROS, reactive oxygen species; THB, 1,2,3-trihydroxylbenzene.

cursor protein by α- and β-secretases produces the $A\beta_{1-16}$ fragment of amyloid precursor protein (15). These soluble fragments and intra-membrane spanning fibrils still possess possible metal binding sites such as histidines, glutamate, aspartate, and tyrosine within the 1–20 fragment of Aβ in the sequence ^{1}DAEFRHDSGYEVHHNKLVFF^{20}. Redox chemistry of Aβ has been previously reported, wherein Met^{35} was suggested as a "built-in" reducing agent required for the redox cycling hypothesis (16). The lack of sufficient data on the redox chemistry of and the oxidative stress caused by metallo-Aβ and the discrepancies in previous studies such as the presence or absence of free-radicals and the nature of the metal-Aβ interaction seem often to be the shortcoming in Aβ research. Understanding of the chemical processes associated with metallo-Aβ may provide insight into the upstream and/or downstream regulatory processes that lead to AD. Herein, we describe the oxidation chemistry of $CuA\beta$ in the presence and absence of H_2O_2, showing conclusive metal-centered pre-equilibrium kinetics toward the oxidation of a simple substrate and the oxidative cleavage of double-stranded plasmid DNA.

MATERIALS AND METHODS

The 1–20 and 1–16 fragments of Aβ were purchased from Sigma-Aldrich or synthesized at the Peptide Center of the University of South Florida. The identities of the peptides have been confirmed with a Bruker matrix-assisted laser desorption ionization time-of-flight mass spectrometer. The substrate 1,2,3-trihydroxylbenzene (THB) and all buffers were obtained from Sigma-Aldrich; 3-methyl-2-benzothiazolinone hydrazone hydrochloride monohydrate from Acros (Fairlawn, NJ); the plasmid pQE30Xa was from Qiagen (Valencia, CA); EDTA, Me_2SO, mannose, H_2O_2, $Cu(NO_3)_2$, $ZnCl_2$, and $NiSO_4$ were from Fisher (Swanee, GA); and $CoCl_2$ was from Mallinckrodt (Paris, KY). All plastic ware was demetallized with EDTA and extensively rinsed with 18-MΩ water to remove the chelator. The water used for the studies of DNA cleavage was autoclaved to remove ubiquitous nucleases.

DNA Cleavage Assay—The metal derivatives of Aβ were prepared by dissolving the peptide in 18-MΩ water and separated into aliquots followed by addition of corresponding metal ions at 1:1 stoichiometric ratio, which was further diluted into aliquots of working concentrations. The derivatives were freshly prepared in all experiments. A typical reaction contained 150 ng of plasmid DNA, 4.0%, 2.0%, or 0.2% H_2O_2, and 5.0 μM of metallo-Aβ derivatives in 100 mM HEPES at pH 7.00 in a volume of 15.0 μl. A time-course experiment was performed, and results were analyzed in a 1.0% agarose gel stained with ethydium bromide and then photographed on a transilluminator.

Catechol Oxidase (THB Oxidation) Assay—Several concentrations of THB ranging from 0.10 to 5.0 mM were incubated with 7.5 μM of $CuA\beta$ and 1.60, 3.20, 16.2, 32.3, or 70.0 mM H_2O_2 and buffered with 100 mM HEPES at pH 7.00 in a final volume of 1.0 ml. The formation of product was monitored at 420 nm (ϵ = 4,583 M^{-1} cm^{-1}) on a Varian CARY50 Bio-UV-Vis spectrophotometer for 5 min, and the rates were determined by the change in absorbance over time. The background oxidation of THB was conducted in the same manner without $CuA\beta$ in the assay solution. Rates were fitted to appropriate rate laws and rate constants determined by the use of SigmaPlot 8.0.

The dependence of H_2O_2 on THB oxidation by $CuA\beta$ was determined by measuring the oxidation rate at several different concentrations of hydrogen peroxide in the presence of 6.0 mM THB. The initial rates were determined and then fitted as a function of $[H_2O_2]$ to an appropriate rate law to reveal the rate constants.

The catechol oxidase assay was also performed as previously reported with minor changes to fit current studies (17). The same molar concentrations of THB and 3-methyl-2-benzothiazolinone hydrazone (which serves as an *ortho*-quinone indicator) were mixed in 100 mM HEPES at pH 7.00 in the presence of 3.5 μM $CuA\beta$. The red adduct of the *ortho*-quinone product was monitored at 500 nm (ϵ = 32,500 M^{-1} cm^{-1}), and rates were calculated. The auto-oxidation rate of THB was determined under the same conditions in the absence of $CuA\beta$.

Metal Titration—Apo-Aβ was dissolved in 100 mM HEPES at pH 7.00 to a final concentration of 1.0 mM. Cu^{2+} binding was monitored by titrating the metal into the apo-Aβ solution, and the electronic spectra were collected after each addition of the metal. Cu^{2+} binding was also determined through the oxidative activity of $CuA\beta$ complex toward THB. In this case, Cu^{2+} was titrated into a fixed amount of the peptide in 100 mM HEPES at pH 7.00 in the presence of 10.0 mM of THB and 70.0 mM H_2O_2. The oxidation rates were determined as a function of $[Cu^{2+}]$, then fitted to a simple equilibrium of metal:peptide = 1:1 or a cooperative binding pattern using the Hill equation.

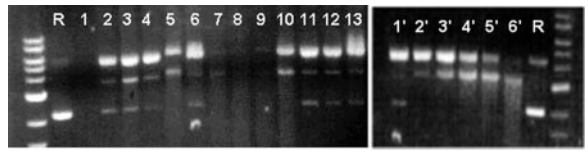

FIG. 1. **Concentration- and metal-dependent assay of dsDNA cleavage.** *R* is the reference plasmid DNA, which shows a supercoiled band (*bottom*) and a nicked circular band (*top*); *lane 1*, DNA plus H_2O_2; *lane 2*, DNA plus $A\beta_{1-20}$ (200 μM) plus 4% H_2O_2; *lanes 3–6*, $ZnA\beta_{1-20}$ (40, 80, 100, and 200 μM, respectively) plus 4% H_2O_2; *lanes 7–13*, $NiA\beta_{1-20}$ (5, 10, 20, 40, 80, 100, and 200 μM, respectively) plus 4% H_2O_2; $CuA\beta_{1-20}$ (at 5, 10, 20, 40, 80, 100, and 200 μM) plus 4% H_2O_2 shows complete DNA cleavage ("blank" gel, not shown). All assays were incubated for 30 min. The middle band is the linearized plasmid detected at the 3.5-kbp position, consistent with that obtained from the sequence of the plasmid pQE30Xa (Qiagen). *Lanes 1′-6′* show the plasmid cleavage by Cu^{2+} ions (5 μM) plus 3.6% H_2O_2 at 10, 20, 40, 60, 90, 120 min. The standard DNA ladder starts with 1 kbp from the bottom with 1-kbp increments upward.

NMR Spectroscopy—All the NMR spectra were acquired on a Bruker DPX250 spectrometer at ^{1}H resonance of 250 MHz. The metal binding was monitored through the changes in the NMR spectra. The peptides $A\beta_{1-16}$ and $A\beta_{1-20}$ and the paramagnetic shift reagent Co^{2+} were prepared in d_6-Me_2SO. The metal ion was gradually titrated into the peptide, and the paramagnetically shifted ^{1}H NMR signals were detected. A typical spectrum of a ~2 mM sample showing the paramagnetically shifted ^{1}H NMR signals consists of ~80,000 transients from accumulation of several spectra of 10,000–20,000 transients with a recycle time of ~50 ms and a spectral window of ~250 ppm. Solvent-exchangeable signals were determined by adding a drop (~25 μl) of D_2O into the sample, which disappear after the addition.

Molecular Mechanics—The primary sequence of $A\beta_{1-16}$ peptide was entered into BioCAChe 6.0 (Fujitsu, Beaverton, Oregon), and the energy of its structure under solvation using a simulated water droplet was minimized with the MM3 molecular mechanics method. Histidine side chains were considered the ligands in the calculations on the basis of the NMR data.

RESULTS AND DISCUSSION

Oxidative Double-stranded DNA Cleavage—Although the bulk of the amyloid plaques in AD brain is membrane-bound, proteolytic processing of amyloid has been shown to yield soluble fragments (13). It has also been demonstrated that the neuropathology of AD may directly affect DNA, eventually leading to apoptosis (18). As metal ions are involved in the formation of amyloid plaques, the oxidative activity of metallo-Aβ derivatives against plasmid DNA was probed *in vitro* with gel electrophoresis. The oxidative activities of the Zn^{2+}, Ni^{2+}, and Cu^{2+} complexes of $A\beta_{1-20}$ ($ZnA\beta_{1-20}$, $NiA\beta_{1-20}$, and $CuA\beta_{1-20}$) toward the cleavage of plasmid DNA were determined by incubating several different concentrations of the complexes with plasmid DNA in the presence of 4.0% H_2O_2 at room temperature for 30 min (Fig. 1). Here, $ZnA\beta_{1-20}$ serves as the control, because Zn^{2+} is oxidative inactive. The plasmid in the presence of metallo-$A\beta_{1-20}$ at lower concentrations shows a middle band that is not present in the reference (*lane R*, Fig. 1). Comparing the middle band with the DNA markers gives an approximate size of 3.5 kbp, consistent with the size of linearized plasmid from the manufacturer. The activities of the derivatives follow the trend $CuA\beta_{1-20} > NiA\beta_{1-20} > ZnA\beta_{1-20}$, demonstrating the involvement of metal in the oxidative cleavage of double-stranded (ds) DNA.

One interesting result is shown in the H_2O_2 plus DNA and the H_2O_2 plus DNA plus $A\beta_{1-20}$ control experiments. An amount of 4.0% H_2O_2 shows a significant damage toward plasmid dsDNA (*lanes 1*, Fig. 1), whereas $A\beta_{1-20}$ decreased the H_2O_2 damage of plasmid dsDNA and perhaps acted as a scav-

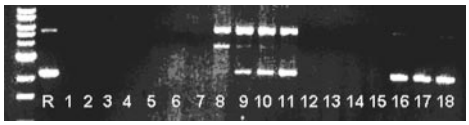

FIG. 2. **Time course reactivity assay of dsDNA cleavage.** *R* is the reference plasmid DNA; *lanes 1–7*, DNA plus 5.0 μM $CuA\beta_{1-20}$ plus 2% H_2O_2 (60, 50, 40, 30, 20, 10, and 5 min, respectively); *lanes 8–11*, DNA plus $A\beta_{1-20}$ (metal free) plus 2% H_2O_2 (60, 40, 20, and 10 min, respectively); *lanes 12–15*, DNA plus 2% H_2O_2 (60, 40, 20, and 10 min, respectively); and *lanes 16–18*, DNA plus $A\beta_{1-20}$ (metal free, peroxide free). The standard DNA ladder starts with 1 kbp from the bottom with 1-kbp increments upward.

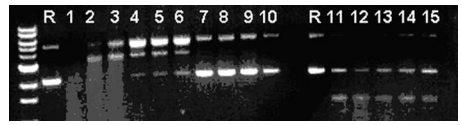

FIG. 3. **Time course reactivity assay toward the cleavage of 150 ng of dsDNA.** *R* is the reference DNA; *lanes 1–6*, DNA plus 5.0 μM $CuA\beta_{1-20}$ plus 0.2% H_2O_2 (60, 40, 30, 20, 15, and 10 min, respectively); *lanes 7–10*, DNA plus 5.0 μM $CuA\beta_{1-20}$ (peroxide free 60, 40, 20, and 10 min, respectively); and *lanes 11–15*, DNA plus 0.2% H_2O_2 (40, 30, 20, 15, and 10 min, respectively). The standard DNA ladder starts with 1 kbp from the bottom with 1-kbp increments upward. The cleavage of plasmid by 5.0 μM Cu^{2+} ions and 3.6% H_2O_2 is shown in Fig. 1, which exhibits a much lower activity.

enger of ROS species (*lane 2*, Fig. 1). The role of Aβ as an antioxidant has been previously reported (19), wherein the presence of Met_{35} was proposed to prevent lipid peroxidation, whereas the M35L mutant showed reduced antioxidant activity. In a similar study, $A\beta_{1-40}$ was found to prevent the oxidation of the lipoproteins from cerebral spinal fluid and plasma (12). Moreover, $A\beta_{1-42}$ was shown to exhibit an antioxidant activity more effective than ascorbic acid in cerebral spinal fluid (20). The antioxidant activity of Aβ was also demonstrated in the decrease of cytoplasmic amounts of 8-hydroxyguanosine, a major product of nucleic acid oxidation present in elevated amounts in the brains of AD patients (21). These observations implied that the production of Aβ could be related to prevention of oxidative stress. We have demonstrated here that even shorter fragments of Aβ without a Met can serve as a protective agent against oxidative damage of DNA, corroborating with some previous reports (12, 20, 21) and supporting the hypothesis that apo-Aβ might be an effect of the oxidative stress in AD brains and might serve a specific purpose to protect from any damage by ROS. This antioxidant activity is also observed in all concentrations of $ZnA\beta_{1-20}$ (*lanes 3–6*, Fig. 1), consistent with the lack of redox chemistry of Zn^{2+} and a protection role against dsDNA cleavage as in the case of apo-$A\beta_{1-20}$.

Although Ni^{2+} is redox active and some of its complexes have been shown to exhibit oxidative damage toward DNA (22), $NiA\beta_{1-20}$ does not show such "chemical nuclease" activity, probably attributed to its low redox potential. Conversely, like apo-Aβ and $ZnA\beta_{1-20}$ discussed above, $NiA\beta_{1-20}$ shows a concentration-dependent *protection* against oxidative damage of dsDNA by H_2O_2, with better protection at higher concentrations while no significant protection at $[NiA\beta_{1-20}] < 80$ μM (*lanes 7–12*, Fig. 1). NiAβ has not been shown to be associated with AD pathology; however, it may serve as a structural and mechanistic probe in future studies of metallo-Aβ or similar systems.

The activity of 5.0 μM $CuA\beta_{1-20}$ is exceedingly higher than that of $ZnA\beta_{1-20}$ at all concentrations tested in the presence of 4.0% H_2O_2 (*lanes 3–6*, Fig. 1), which effectively oxidizes the entire dsDNA plasmid sample into fragments that are too small to be resolved with the agarose gel electrophoresis (empty lanes not shown). Cu^{2+} ion has been demonstrated in the literature to be active toward DNA cleavage in the presence of H_2O_2 (23–27). The use of Cu^{2+} (5.0 μM) in the presence of 3.6% H_2O_2 as control shows a much slower cleavage rate as the plasmid is not completely digested after 2 h of incubation (*lanes 1′–6′*). To monitor the catalytic activity of $CuA\beta_{1-20}$ toward plasmid dsDNA, the concentration of H_2O_2 was reduced to 2.0% and a time course experiment conducted (Fig. 2). $CuA\beta_{1-20}$ completely oxidizes plasmid DNA within 5.0 min in the presence of 2.0% H_2O_2, leaving only a faint streak in the gel (*lane 7*, Fig. 2). The ability of apo-$A\beta_{1-20}$ to act as a protector against oxidation of dsDNA in the presence of H_2O_2 is once again demonstrated here. Further reducing the concentration of H_2O_2 to 0.2% allows a clearer monitoring of plasmid cleavage patterns (Fig. 3). Within 10 min of incubation, 5.0 μM of $CuA\beta_{1-20}$ shows double-stranded DNA cleavage as evident in the appearance of a middle band ~3.5 kbp (*lane 6*, Fig. 3). Within 20–30 min, complete conversion of the supercoiled plasmid into linear and nick-circular conformations is observed, evident in the changes in the intensity of the different forms of the plasmid compared with the reference (*lanes 3* and *4*, respectively, Fig. 3). After 30 min, plasmid is cleaved into small pieces leaving a streak of oligonucleotide products (*lanes 1–3*). The different and quite opposite activities between apo-$A\beta_{1-20}$ and $CuA\beta_{1-20}$ toward dsDNA damage may hint a physiological role of small fragments of apo-Aβ.

To determine the role of the oxidizing agent in these reactions, the same concentration of $CuA\beta_{1-20}$ was incubated with the plasmid in the absence of H_2O_2 up to 60 min, which shows negligible cleavage (*lane 7*, Fig. 3). The low activity of $CuA\beta_{1-20}$ without H_2O_2 indicates a metal-centered activation of peroxide, such as the formation of a Cu_2-peroxo center found in many copper complexes (28–30), which subsequently results in oxidative damage to dsDNA. To distinguish the reaction pathways of oxidative DNA cleavage by H_2O_2 in the presence and absence of $CuA\beta_{1-20}$, a time-course experiment was established (*lanes 11–15*, Fig. 3). The reaction patterns of dsDNA cleavage in these two cases are clearly different. In the absence of $A\beta_{1-20}$, dsDNA is cleaved into small fragments without formation of a linear intermediate as evident by the faint band at 2.0 kbp. The nature of the band is not clear at this stage and is not associated with Aβ. The dsDNA cleavage by $CuA\beta_{1-20}$ in the presence of H_2O_2 is conformation-dependent, most active toward supercoiled dsDNA as evident by the accumulation of nicked-circular and linear forms with time in the reaction, likely due to the structural constraints of the supercoiled form. The accumulation of the linearized form (middle bands) is indicative of double-stranded DNA cleavage, rather than a random single-stranded cleavage, which is a key trigger that can result in cell apoptosis (31). The linearization of the plasmid via cleavage of dsDNA is also characteristic of the cleavage pattern by DNA-recognizing agents such as Cu-bleomycin (32).

False regulation of metal homeostasis and ROS physiology is closely related to aging and oxidative stress (7), wherein apo-$A\beta_{1-20}$ seems to serve as a scavenger of metal ions due to its large affinity constant with metal ions and a protective agent against oxidative damage of biological macromolecules by H_2O_2 based on the observations in this and other studies (33, 34). However, the presence of H_2O_2 can result in severe damage toward dsDNA and presumably other redox-sensitive biomolecules as well by metallo-Aβ when the metal ions are redox active as demonstrated herein.

The mechanism of oxidative "chemical nucleases" has been thoroughly studied and reviewed (35). According to the studies of some simple chemical nucleases such as Cu-1,10-phenanthroline, a reduced state of the metal center (by a reducing agent) is required for catalysis in the presence of O_2. In our

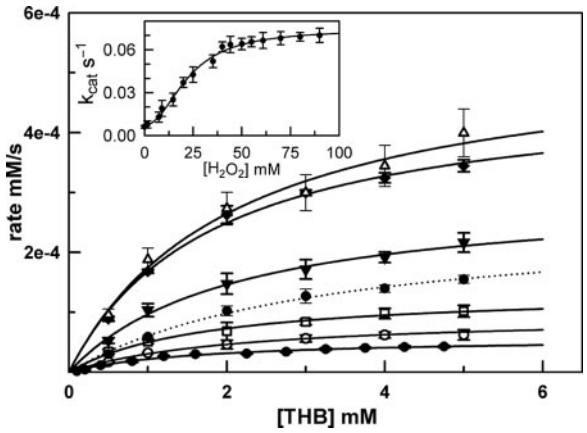

FIG. 4. **Effect of peroxide concentrations on the rate of THB oxidation in the presence of 7.5 μM of CuAβ$_{1–20}$ in the presence of 1.6 (●), 3.2 (○), 16.2 (□), 32.3 (▼), 64.6 (◇), and 70.0 (△) mM H_2O_2 (HEPES buffer of 100 mM at pH 7.0 and 25.0 °C).** The *dotted line* is CuAβ$_{1–16}$ in the presence of 16.2 mM H_2O_2. The *inset* shows the first order rate constant k_{cat} as a function of hydrogen peroxide, wherein the *solid trace* is a fitting of the data to the Hill equation by taking into consideration of an activity at 0% H_2O_2.

experiments, however, the absence of a reducing agent to convert Cu^{2+} to Cu^{+} and the use of H_2O_2 as the oxidation agent suggest a different oxidative pathway. Moreover, the free radical scavenger (36) Me_2SO did not inhibit the reaction, suggesting the absence of free radicals to induce the oxidative damage. On the basis of the results shown here, we propose a peroxo-bridged dinuclear Cu^{2+} active center for CuAβ$_{1–20}$ as observed in a number of dinuclear chemical model systems (28) and in catechol oxidase, tyrosinase, and hemocyanin (37, 38). The nature of this transient peroxo-bridging species and its attack on the substrates, although thoroughly studied, still has key mechanistic questions to be answered, such as the true structure of reaction intermediates, the role of substrate in the reaction mechanism, rate determining steps in catalysis, and specificity of metal cofactor for the function of enzymes like catechol oxidase, tyrosinase, peptidylglycine monooxygenase, methane monooxygenase, fatty acid desaturase, and ribonucleotide reductase (39–41). It has been proposed that substrate accessibility in the active site after O_2 binding plays a key role in the action of these proteins (39, 42). Consequently, a reversible O_2 binding has been demonstrated in hemocyanin because of the lack of substrate accessibility, wherein bulky substrates such as aromatic systems and the ribose moiety of DNA may not easily gain access to the O_2-binding active center of the proteins. However, studies of catechol oxidase and tyrosinase have shown the production of hydroxylated phenols and *ortho*-quinones, reflecting that substrates bind directly to the dinuclear peroxo-Cu_2 active center, which enables a direct attack on the substrates by the peroxo unit (29, 30, 43).

Kinetics and Mechanism of Oxidative Catalysis by CuAβ—To gain further insight into the mechanism for the oxidation activity of CuAβ$_{1–20}$ and its interaction with H_2O_2, the catechol analogue 1,2,3-trihydroxylbenzene (THB) was utilized to provide detailed kinetic information owing to its easily accessible oxidation state, which also has been utilized for investigation of oxidative activities of metal complexes (44). The oxidation rate of THB by 7.5 μM CuAβ$_{1–20}$ was determined at different values of [THB] in the presence of H_2O_2 at various concentrations (Fig. 4), which reached saturation at high THB concentrations. This saturation pattern suggests a possibility of metal-centered pre-equilibrium kinetics. The rate law for this reaction mechanism can be expressed as in Equation 1,

$$V_0 = v_{\text{backgrond}} + \frac{k_{\text{cat}}[\text{CuA}\beta][\text{THB}]}{K'_{\text{app}} + [\text{THB}]} \qquad \text{(Eq. 1)}$$

assuming that the concentration of the intermediate THB·CuAβ$_{1–20}$ complex is much lower than that of the unbound THB in which $K'_{app} = (k_{-1} + k_{cat})/k_1$ is the virtual dissociation constant, and k_1 and k_{-1} are the rate constants for the formation and dissociation, respectively, of the THB·CuAβ$_{1–20}$ complex. The data can be well fitted to Equation 1, yielding k_{cat} = 0.00767 s^{-1} and K'_{app} = 1.67 mM, and a second-order rate constant k_{cat}/K'_{app} of 4.59 M^{-1} s^{-1} for the reaction in the presence of 16.0 mM (0.0544%) H_2O_2. This represents a 724-fold increase in terms of the first-order rate constant when compared with the auto-oxidation of THB under the same reaction conditions in the absence of CuAβ$_{1–20}$ (determined to be k_0 = 1.06×10^{-5} s^{-1}). A plot of k_{cat} as a function of $[H_2O_2]$ from Fig. 4 shows that k_{cat} reaches a plateau at high H_2O_2 concentrations (*inset*, Fig. 4). However, the k_{cat} value does not reach zero at 0% H_2O_2, which is higher than k_0 of the auto-oxidation of the substrate. The oxidation reaction in the absence of H_2O_2 was further explored and discussed in a later section below. The plot seems slightly sigmoidal, which indicates a possible presence of either a consecutive or a cooperative binding of H_2O_2 to the active center. Because catechol oxidation involves 2-electron transfer, which matches the two-electron reduction of H_2O_2 to yield two oxides, a consecutive mechanism is not fundamentally necessary for the reaction to take place. The data were fitted to the Hill equation (*inset*) to extract the Hill coefficient θ of 2.09 and k_{cat} value of 0.00731 s^{-1} at 0% H_2O_2 (close to the value of 0.0065 s^{-1} directly measured in the absence of exogenous H_2O_2 discussed later), indicative of the presence of weak cooperativity and H_2O_2-independent oxidative catalysis. Interestingly, the smaller fragment CuAβ$_{1–16}$ showed more than 4-fold higher k_{cat} of 0.0340 s^{-1} for the reaction with the same concentration of H_2O_2 (Fig. 4). However, its catalytic efficiency is only twice higher than the larger fragment in terms of the second order rate constant k_{cat}/K'_{app} (10.5 M^{-1} s^{-1}), which suggests a participation of the last four C-terminal hydrophobic residues (LVFF) in the reaction pathway. The hydrophobic C terminus may influence substrate binding and product release as reflected by the higher K'_{app} and k_{cat} values for CuAβ$_{1–16}$ (K'_{app} = 3.23 mM). This observation suggests that the C terminus is able to influence THB binding and/or a transition-state conformational change that affects both the binding of THB and the turnover of the reaction.

It has previously been documented that H_2O_2 and other ROS generated by metallo-Aβ may play a role in the pathology of AD (33, 34, 45). Because the local concentration of metallo-Aβ in an AD brain can reach sub-millimolar range (8), the above observation implies that a significant rate acceleration in redox reactions can be expected at a location where H_2O_2 is produced. This rate enhancement in the brains of AD patients can be metabolically catastrophic. In the studies shown here, we have further specified the fate of H_2O_2 in metallo-Aβ-associated redox reactions.

To further analyze the role of H_2O_2 in the reaction pathway, a saturation profile was constructed with a fixed amount of the substrate THB at 6.0 mM. Under such conditions, the reaction reaches plateau at $[H_2O_2]$ near 70.0 mM or 0.238% (Fig. 5). The results can be well fitted to a pre-equilibrium kinetics (Equation 2). This kinetics further corroborates a metal-centered mechanism.

$$V_0 = v_{\text{background}} + \frac{k_{\text{cat}}[\text{CuA}\beta][\text{H}_2\text{O}_2]}{K'_{\alpha\text{app}} + [\text{H}_2\text{O}_2]} \qquad \text{(Eq. 2)}$$

The rate of acceleration against the background oxidation of THB under the same conditions in the presence of $[H_2O_2]$ is

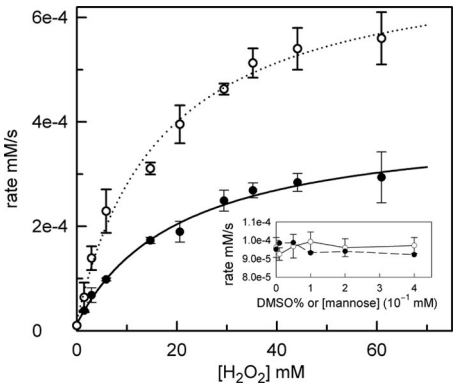

FIG. 5. **H_2O_2 saturation profile of CuAβ_{1-16} (○) and CuAβ_{1-20} (●) activity at a fixed [THB] of 6.0 mM (HEPES buffer of 100 mM at pH 7.0 and 25.0 °C).** The *inset* shows that Me_2SO (*DMSO*, ○) and mannose (●) do not inhibit the oxidation of THB by CuAβ.

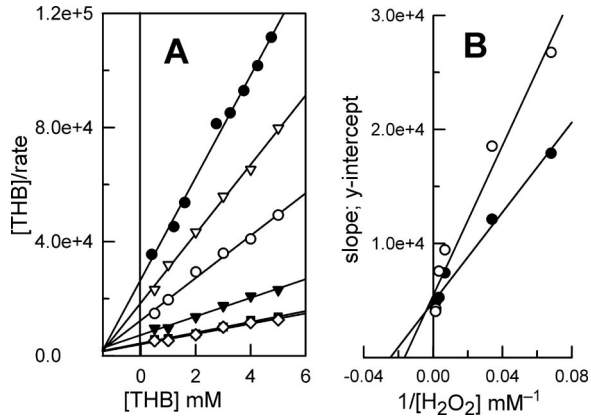

FIG. 6. **Hanes analysis of the kinetic data from Fig. 4.** The plots in *A* yield the apparent virtual dissociation constant for THB. The re-plot of the slope and *y*-intercept from *A versus* $1/[H_2O_2]$ reveals (in *B*) true dissociation constants for THB (0.41 mM) and H_2O_2 (17.3 mM) in a bi-substrate reaction.

~6000-fold (background rate constant measured to be $k_o = 1.14 \times 10^{-5}\ s^{-1}$) with $k_{cat} = 0.066\ s^{-1}$ and $k_{cat}/K'_{app} = 37.2\ M^{-1}\ s^{-1}$. The hydrophobicity at the C terminus does not affect the binding of H_2O_2 as reflected by the similar apparent virtual dissociation constant K'_{app} between CuAβ_{1-20} and CuAβ_{1-16} (17.3 and 16.6 mM, respectively). Qualitatively, because the k_{cat} value is small, the K'_{app} value is expected to be closer to the dissociation of the CuAβ·THB complex. The binding of each H_2O_2 molecule thus may have a large dissociation constant, suggesting that formation of the intermediate Cu-peroxo active center is not favorable under the experimental conditions, which may well be the rate-determining step. This result corroborates with chemical model studies of catechol oxidase and tyrosinase in that a dinuclear Cu-peroxo intermediate is often short-lived and thermodynamically unstable (29, 30, 46).

Because the involvement of free radicals in the redox chemistry of metallo-Aβ had been implicated in previous reports (8), different amounts of Me_2SO and mannose, two common scavengers for superoxide free radical and hydroxyl free radical (36, 47) were added to the reaction solution separately with saturating concentrations of H_2O_2 and THB. No noticeable effect on the reaction rates was observed under the experimental conditions (Fig. 5, *inset*), corroborating what was observed in the plasmid DNA cleavage study discussed above. However, this does not discount possible free radical generation, because the free radicals may well be metal-centered and free-radical oxidation in solution may not be the predominant pathway in the oxidation of THB catalyzed by CuAβ_{1-20}. We have established here a metal-centered oxidative catalysis by CuAβ_{1-20} and CuAβ_{1-16} that cannot only generate H_2O_2 as noted previously (45) but also activate H_2O_2 for possible oxidation of biomolecules,[2] clearly demonstrating the fate of H_2O_2 in this AD-related system.

Because both H_2O_2 and THB can interact with the metal center and are considered "substrates" for CuAβ, it is imperative to further narrow down the mechanism about how these two substrates interact individually with the metal center. For this purpose, the redox indicator 3-methyl-2-benzothiazolinone hydrazone was used to probe the oxidation product of THB *in the absence of H_2O_2*. 3-Methyl-2-benzothiazolinone hydrazone is a common indicator used in catechol oxidase assay that forms a red adduct with the *o*-quinone products instantaneously (17). The rate for the oxidation of a catechol into its corresponding *o*-quinone can thus be easily monitored colorimetrically as the oxidation is the rate-limiting step. The rate for the oxidation of THB by CuAβ_{1-20} in the absence of H_2O_2 as a function of [THB] is not linear, which can be well fitted to pre-equilibrium kinetics to give $k_{cat} = 0.0065\ s^{-1}$ (consistent with the value at 0% H_2O_2 obtained from the k_{cat} *versus* $[H_2O_2]$ plot, Fig. 4, *inset*) and $K'_{app} = 2.0$ mM. The first order rate acceleration of THB oxidation here is 650-fold with respect to the auto-oxidation (*i.e.* k_{cat}/k_o; k_o was measured to be $1.06 \times 10^{-5}\ s^{-1}$). This oxidative reaction is much less significant in terms of rate acceleration than that in the presence of a saturating amount of H_2O_2 described above. Here, THB is possibly oxidized by CuAβ in form of a dinuclear Cu^{2+} center via 2-electron transfer to afford $2Cu^+$ and *o*-quinone product. The reduced $2Cu^+$ in turn can bind O_2 to form a dinuclear Cu^{2+}-peroxo center and follow the catalytic pathway as the CuAβ/H_2O_2 system discussed above.

Because a bi-substrate mechanism was implied from our results (*i.e.* both THB and H_2O_2 show saturation), further analysis of the data was performed. The Hanes analysis was used to minimize the error across the concentration range (Fig. 6*A*) (48). The virtual dissociation constant K'_{app} for both substrates cannot be resolved only from the primary nonlinear fitting without analyzing their combined effects (49). It is thus important to determine the rates at varying amounts of H_2O_2 when holding THB constant and *vice versa*. The data in Fig. 4 were fitted to a two-substrate random-binding mechanism according to Equation 3 (Fig. 6*A*) (48),

$$\frac{[THB]}{V_0} = \frac{(1+(K'/[H_2O_2]))}{V_{max}}[THB] + \frac{K'_\alpha}{V_{max}}(1+(K_i/[H_2O_2])) \qquad \text{(Eq. 3)}$$

wherein the binding of THB and H_2O_2 to CuAβ_{1-20} was assumed to be random and in rapid-equilibrium with a subsequent ordered product release. Under these conditions, a simple conversion to a secondary plot of the slope ($1/V_{max}$) and the *y*-intercept (K'_{app}/V_{max}) obtained from Fig. 6*A* *versus* $1/[H_2O_2]$ yields K' and K'_α, the true values for the virtual dissociation of THB and H_2O_2, respectively, and the product inhibition constant K_i (Fig. 6*B*). Moreover, if any cooperativity is present in this bi-substrate reaction mechanism, it would be revealed by the ratio of K'_{app}/K'. For a random equilibrium mechanism a ratio of K'_{app}/K' between 1 and 5 would suggest small cooperativity (49). In the oxidative catalysis by CuAβ_{1-20}, the K'_{app}/K' ratio is 2.85 for THB oxidation and $K'_{\alpha app}/K'_\alpha$ is 1.62 for H_2O_2, which indicates small cooperativity. It is important to note that based on the data alone it is difficult to distinguish between an ordered sequential-binding mechanism and the mechanism herein proposed (48). However, a random equilibrium phase is

[2] Preliminary results from our studies show effective oxidations of a few catecholamines by CuAβ in the presence of H_2O_2.

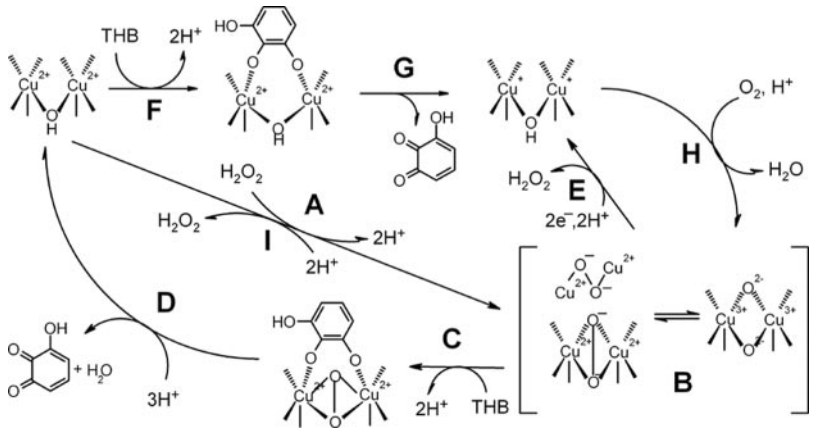

FIG. 7. **Proposed mechanism for the oxidation of THB by CuAβ in the presence (*steps A–D*) and absence of H_2O_2 (*steps F–H* and *B–D*).** The production of H_2O_2 under reduction conditions (*step E*) is also consistent with this mechanism.

a sound assumption, because both THB and H_2O_2 can interact with the metal centers separately.

In our proposed reaction mechanism, only when both THB and H_2O_2 substrates bind to the metal-center can productive turnover be observed with second-order rate constants of 8.66 and 15.6 M^{-1} s^{-1} for the oxidation of THB by CuAβ_{1-20} and CuAβ_{1-16}, respectively, in the presence of H_2O_2 (whereas molecular O_2 serves as the second substrate in the absence of H_2O_2). This pathway differs from the previously proposed mechanism in the redox cycling of metallo-Aβ wherein the presence of the thioether group of Met^{35} was accounted for the reduction of the metal center (19). The results presented here indicate substrate-mediated reduction of the metal center (because Met is absent in the studies) as well as oxidation of the substrate by metal-activated H_2O_2. However, our data do not discount the possibility of the involvement of Met in the reductive pathway in A$\beta_{1-40/42}$. Regardless, the redox chemistry of CuAβ presented here shows an important mechanism for possible destructive actions in Alzheimer's disease.

Taken together, the metal-centered redox cycle of CuAβ action in this study seems to match the mechanism of the dinuclear Cu-containing catechol oxidase, wherein the oxidation of the substrate takes place both in the presence and absence of H_2O_2 (37, 38). Because the oxidation of catechols is a two-electron transfer process, the involvement of a dinuclear copper center is thus a preferred pathway as in the case of the enzyme. In the presence of THB and H_2O_2, the dinuclear μ-η^2:η^2-peroxo-Cu_2^{2+}-THB transition state is eventually formed by assembling two metal centers together via the bridging peroxo (Fig. 7, *steps A–C*) as in the case of many mononuclear Cu^{2+} complexes (28–30), which is followed by 2-electron transfer from the bound catechol to the bound peroxide (likely through the metal center) to yield Cu_2^{2+}-μ-OH and *o*-quinone to complete a catalytic cycle (*step D*). Here, the dinuclear centers oxy-$Cu^{+}{}_2$ μ-η^2,:η^2-peroxo-Cu_2^{2+} μ-η^1,:η^1-peroxo-Cu_2^{2+}, and (μ-oxo)$_2$-Cu_2^{3+} (B) are isoelectronic (29, 30) and were not distinguishable in our study. In the absence of H_2O_2, the oxidation of the bound THB is achieved by 2-electron transfer to the dinuclear Cu_2^{2+} center to yield $Cu^{+}{}_2$ (*steps F* and *G*), which is followed by O_2 and THB binding to regenerate the μ-η^2:η^2-peroxo-Cu_2^{2+}-THB transition state (*steps H*, *B*, and *C*). The binary and the ternary complexes then follow the same pathway as the case in the presence of H_2O_2 for another turnover. H_2O_2 is also generated according to this mechanism under reducing and acidic conditions (*steps E* and *I*), which have been previously observed (45) and can serve as a competing reaction pathway toward the oxidation of catechols (*steps C* and *D*).

Metal Binding and Structure—Detailed information about the metal-binding ligands and geometry of the metal site is needed to gain further insight into the metal-centered redox chemistry and to elucidate any structure-function correlation important for the action of metallo-Aβ. Because activity is an excellent probe for monitoring reaction mechanism, it is thus chosen as a probe for the determination of the metal-binding stoichiometry of metallo-Aβ. Upon introduction of Cu^{2+} to Aβ, oxidative activity can be measured as described above. It is evident from the data that metal binding reaches saturation at slightly above 1:1 ligand-to-metal ratio (Fig. 8). Despite a previous electron paramagnetic resonance study that indicates the binding of two Cu^{2+} ions to Aβ (50), our result indicates the active species is a 1:1 CuAβ complex. Both a non-cooperative binding equilibrium (a quadratic pattern) and a cooperative equilibrium (a sigmoidal pattern) were used to fit the data. It is evident from the fitting that the shorter CuAβ_{1-16} fits equally well to both binding patterns with a metal-to-ligand stoichiometry of 1 to 1, whereas CuAβ_{1-20} seems to fit better the cooperative binding pattern. The binding of Cu^{2+} to Aβ_{1-16} gives a Hill coefficient θ of 1.94, whereas the binding to Aβ_{1-20} shows a higher cooperativity with θ of 3.27. This result is consistent with previous reports of cooperative metal binding to the entire Aβ determined on the basis of quantitative precipitation (51). The results presented here further indicate the presence of cooperativity in the oxidative activity as well as metal binding. The higher C-terminal hydrophobicity of Aβ_{1-20} may influence intermolecular interactions, resulting in a more apparent cooperativity. The data were also analyzed to determine whether or not there were possible inactive dimer conformations of this metallopeptide by plotting activity as function of the square root of metal ion concentration as previously described (52). However, the data do not reflect the existence of such equilibrium in this reaction pathway, adding supporting evidence to the dinuclear metal-centered redox mechanism herein proposed. Dissociation constants (K_d) for metal binding to Aβ can be extrapolated from both fits with values of 3.96 and 4.30 μM for CuAβ_{1-16} and CuAβ_{1-20}, respectively. Because activity serves as the probe here, the values obtained above are thus the intrinsic dissociation constants attributable to the active CuAβ complexes and are not affected by coagulation equilibrium for Aβ. The intrinsic dissociation constant for metal binding in CuAβ_{1-40} is likely to be in the same range of ~4 μM for CuAβ_{1-20} and CuAβ_{1-16} owing to their probably similar metal-binding configuration. Indeed, dissociation constants in the range of ~0.1 μM for CuAβ_{1-28} and ~2 μM for CuAβ_{1-40} and CuAβ_{1-42} were determined with ligand competition (50) and direct fluorescence measurement (53). An apparent dissociation constant $K_d$app of 0.50 pM for Cu^{2+} binding toAβ_{1-40} was determined based on the formation of CuAβ_{1-40} coagulates (51), which can be dissected into the intrinsic metal dissociation constant K_{Cu} of ~4 μM, and the dissociation constant of CuAβ_{1-40} coagulates K_{co} ~ 0.13 μM (*i.e.* $K_d$app = K_{Cu} × K_{co}).

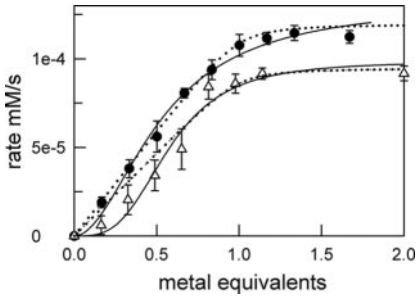

FIG. 8. **Cu^2 titration to $A\beta_{1-20}$ (▲) and $A\beta_{1-16}$ (●) monitored with their oxidation activities (100 mM HEPES buffer at pH 7.0 and 25.0 °C).** The *dotted curves* show the best fittings to a non-cooperative $M+L \rightleftharpoons ML$ equilibrium. *Solid curves* are the nonlinear fittings to the Hill equation, which yield Hill coefficients of 1.94 and 3.27 for Cu^{2+} binding to $A\beta_{1-16}$ and $A\beta_{1-20}$, respectively.

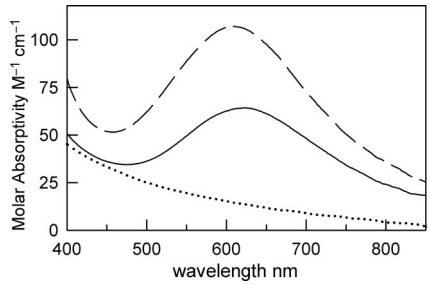

FIG. 9. **Electronic spectra of $A\beta_{1-20}$ with 0.5 equivalents (*solid trace*) and 1.0 equivalent Cu^{2+} (*dashed trace*) referenced against apo-$A\beta_{1-20}$ (100 mM HEPES buffer at pH 7.0).** The *dotted trace* is the difference spectra of 1.4 and 1.0 equivalents of Cu^{+2} in $A\beta_{1-20}$, showing no further increase in the *d-d* transition after the binding of one equivalent of Cu^{2+}.

The much smaller apparent dissociation constant of 6.3 aM for Cu^{2+} binding to $A\beta_{1-42}$ would thus afford the dissociation constant of $CuA\beta_{1-42}$ coagulates in the range of 1.6 pM. A recent report indicates that trace amounts of metal ions can significantly affect Aβ coagulation (54); it is thus suspected that the dissociation constants may be underestimated based on the coagulation. We report herein a direct and reliable means for the determination of metal binding to soluble Aβ fragments that is not complicated by the formation of the coagulation as previously observed (51) that can be influenced by other factors, such as trace amount of metal ions (54).

To further investigate the metal-coordination environment, the electronic spectrum of $CuA\beta_{1-20}$ was obtained (Fig. 9). The spectrum reveals a typical type-2 copper center with *d-d* transitions showing λ_{max} at 610 nm (107 M^{-1} cm^{-1}), clearly distinguishable from the near IR absorption at 820 nm for aqueous Cu^{2+} solutions. This absorption is consistent with that of the "CuH_2L" species of acetyl-$A\beta_{1-16}$ with three coordinated His side chains in a potentiometric study (55) (617 nm and 117 M^{-1} cm^{-1}) and another report (50) (610 nm and ~50 M^{-1} cm^{-1}, which seems to be an absorptivity that is too low (56)). This result agrees well with a tetragonally distorted octahedral environment caused by the Jahn-Teller effect (56, 57) for the d^9 Cu^{2+} in $CuA\beta_{1-20}$. Upon addition of more than one equivalent of metal, the spectrum does not change. This is consistent with the results when activity was used as the probe to monitor metal binding (Fig. 8), wherein one equivalent Cu^{2+} is determined to bind to one peptide. It is also worth noting that there are no intense transitions in the near-UV range that can be possibly assigned to Tyr-to-Cu^{2+} charge-transfer transitions.

The metal coordination chemistry was also investigated by the use of Co^{2+} as an NMR probe. Co^{2+} has been well demonstrated to be an excellent probe for the investigation of metal-binding sites in a number of metalloproteins, including zinc and copper proteins (58, 59). Although $A\beta_{1-20}$ has four additional hydrophobic amino acids on the C terminus, the conformations of the two peptides in d_6-Me_2SO are similar as they show nearly identical ^1H NMR spectra (Fig. 10). The signals due to $^{17}LVFF^{20}$ side chains in $A\beta_{1-20}$ are clearly observed when compared with the spectrum of $A\beta_{1-16}$, wherein LV are seen at ~0.6 ppm and FF ~7.2 ppm. This similarity reflects their similar configuration. There are two solvent-exchangeable signals in the range of 14–16 ppm (imidazole N-H signature chemical shifts (60)) with a 1:2 ratio in intensity, corresponding to the three His side chains (*insets*, Fig. 10). Upon Co^{2+} titration, the intensities of these solvent-exchangeable His-imidazole signals gradually decreased, which was accompanied by the appearance of three far-downfield paramagnetically shifted signals in the region of 40–80 ppm as shown here for $A\beta_{1-20}$ (Fig. 10*C*). These far-shifted signals are also solvent-exchangeable and correspond to the chemical shift of the solvent-exchangeable signal of a paramagnetic Co^{2+}-bound imidazole group of a histidine residue (which cannot result from dipolar shift of unbound His residues, because the octahedral Co^{2+} center is expected not to possess magnetic anisotropy) as observed in many Co^{2+}-substituted metalloproteins (58). These three solvent-exchangeable NH signals further confirms the involvement of all three histidine residues in $A\beta_{1-20}$ for metal binding, consistent with previous Raman spectroscopic studies (10), and is indicative of the absence of a bridging histidyl imidazole (in contrast to what has been previously suggested (10, 13)), which would result in the loss of an imidazole NH signal. Tyr^{10} was suggested to be a possible ligand for Cu^{2+} and Fe^{3+} binding (10, 13, 61), but was suggested not to be a ligand in other studies (55). The ^1H NMR signals of Tyr^{10} (the two doublets with *asterisks* centered at ~6.7 ppm in Fig. 10) do not show any noticeable change upon the addition of the paramagnetic Co^{2+} ion. The binding of a Tyr-phenol group to Co^{2+} is expected to exhibit paramagnetically shifted ^1H NMR signals of the bound phenol group outside the diamagnetic region as previously observed (62). This indicates that this Tyr is not a metal-binding ligand, consistent with the lack of charge-trans-

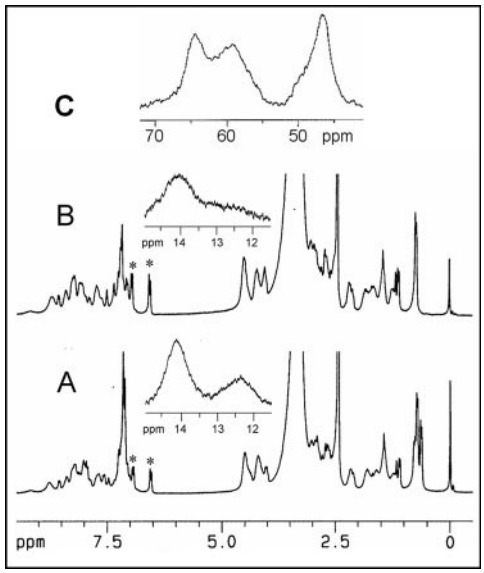

FIG. 10. **^1H NMR spectra of $A\beta_{1-20}$ (*A*) and $A\beta_{1-16}$ (*B*) in d_6-Me_2SO.** The *insets* show the imidazole N-H solvent-exchangeable signals of His, which disappear upon addition of a drop of D_2O (remain intact with same amount of H_2O). These signals disappear upon addition of paramagnetic Co^{2+}, with concomitant appearance of three solvent-exchangeable hyperfine-shifted signals in the far-downfield region as shown here for Co-$A\beta_{1-20}$ (*C*). The signals with *asterisks* in *A* and *B* are due to Tyr ring protons, which remain the same upon Co^{2+} binding.

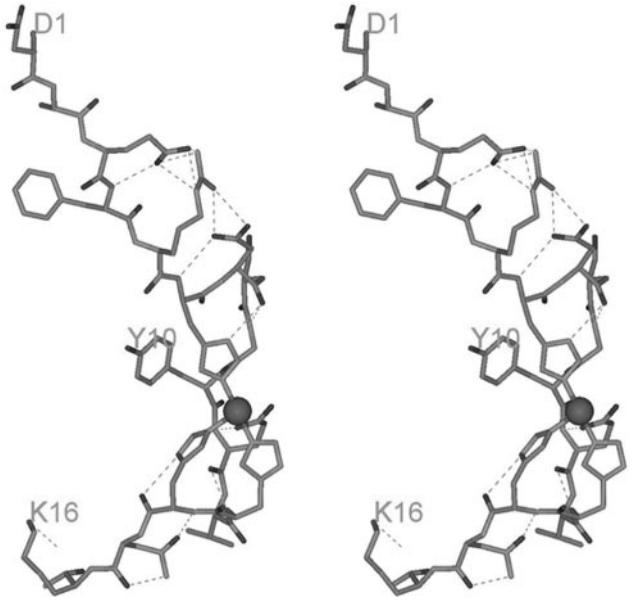

FIG. 11. **Proposed metal coordination and solution structure of CuAβ_{1-16} in a relaxed-eye stereo view based on NMR study of Co^{2+} binding and molecular mechanics calculations.** According to the molecular mechanical calculations both the two-histidine (His^{13}/His^{14}) and three-histidine binding patterns are stable, whereas NMR study suggests the latter binding pattern. The *dotted lines* are H-bonds, which may prevent further bending of the peptide to allow the binding of the N terminus to the metal as recently reported (50).

fer transitions for a possible Tyr-Cu^{2+} binding as described above. Our results also do not support the binding of the N-terminal amino group to the metal as previously suggested (50). This binding mode for paramagnetic Co^{2+} would show far upfield-shifted NH_2 signal(s), a downfield-sifted $C_\alpha H$ proton, and slightly upfield-shifted $C_\beta H_2$ protons owing to spin polarization, which were not observed. Moreover, molecular mechanical calculations also did not support such binding (discussed below).

Molecular mechanical calculations have been applied to determine the structure of Aβ_{1-16} and its metal-binding domain. The energies for different metal-binding modes have been calculated by the use of the MM3 force field and a simulated water droplet to solvate the peptide. Binding of Cu^{2+} to His^{13} and His^{14} yields the lowest energy of −385 kcal/mol as compared with all other possible binding modes in the peptide. The binding to all three His side chains yields a distorted octahedral geometry (with three open coordination sites presumably occupied by water molecules) and a slightly higher energy at −363 kcal/mol (Fig. 11). The energy difference between these two metal-binding modes may be low enough to be easily overcome at room temperature. Extensive H-bonding are observed in this calculated structure, particularly Glu^3-Arg^5-Asp^7 H-bonding interactions may stabilize the structure to a great extent (*dotted lines* in Fig. 11). The energies for Cu^{2+} binding to $His^{6/13}$ and $His^{6/14}$ are much higher at −125 and −210 kcal/mol, respectively, and are not likely to be the metal binding modes for Aβ. A histidine-bridged dimer form of the peptide previously proposed (13) was also calculated, which gave an unacceptably high overall energy of 52,500 kcal/mol. The binding of Tyr^{10} along with the histidine residues is also highly unfavorable, which puts undue stress on the phenol ring causing it to pucker and the peptide backbone to distort, with a high overall energy of 570 kcal/mol. The recently suggested N-terminal binding mode (50) (along with the binding of the three histidines) has also been calculated to give an unfavorable overall energy of 147 kcal/mol. Because Cu^+ can easily adopt a trigonal coordination sphere (57), a calculation with a fixed trigonal coordination was performed that yielded an energy of −318 kcal/mol. The low energy difference between octahedral and trigonal geometries rationalizes the redox cycle of the copper center in the catalysis of catechol oxidation. The binding of the three His side chains to the metal renders one side of the metal center to have an open coordination sphere which can possibly bind H_2O_2 or O_2 to form the peroxo-bridging dinuclear center described above.

Concluding Remarks—The results presented here have added further insight and support to the structure and chemistry of metallo-Aβ which may assist better understanding of the neuropathology of Alzheimer's disease. A complete redox cycle for the action of CuAβ has been proposed from the kinetic studies that is consistent with the mechanism proposed for the dinuclear copper catechol oxidase. The results in this report, however, do not resolve the cause/effect debate about the role of Aβ in AD, but add more information to the chemistry of metallo-Aβ. As a cause for AD, we have shown and quantified redox chemistry of CuAβ that can serve as a catalyst both in the absence and presence of H_2O_2 to cause severe oxidative damages in the brains of AD patients. As an effect of AD, Aβ can be reasoned to be present as a regulator toward metal ion homeostasis due to its considerable metal affinities and its protective property toward oxidative DNA damage in the absence of Cu^{2+}. In the latter case, abnormal homeostasis of redox-active metal ions can leach the metal ions to yield metallo-Aβ, which can undergo redox destruction of biomolecules. We have presented data to revise the redox chemistry of the methionine-centered hypothesis by showing a metal-centered catalysis as a significant contribution to the oxidative damage in the pathology of the neurodegenerative AD. The fate of H_2O_2 generated by CuAβ in the presence of a reducing agent previously observed or an electron-donating substrate shown here has also been established and quantified with exogenous addition of this oxidant. Further studies currently under way that focus on the structure-activity relationship of metallo-Aβ are expected to shed light on the roles of metal ions and Aβ in AD and hopefully will provide useful information for treatment and prevention of Alzheimer's disease.

Acknowledgments—We also thank Dr. Brian Livingston for providing the plasmid and Dr. Ted Gauthier for the syntheses of the peptides in this research.

REFERENCES

1. Paik, S. R., Shin, H. J., Lee, J. H., Chang, C. S., and Kim, J. (1999) *Biochem. J.* **340,** 821–828
2. Paik, S. R., Shin, H. J., and Lee, J. H. (2000) *Arch. Biochem. Biophys.* **378,** 269–277
3. Estevez, A. G., Crow, J. P., Sampson, J. B., Reiter, C., Zhuang, Y., Richardson, G. J., Tarpey, M. M., Barbeito, L., and Beckman, J. S. (1999) *Science* **286,** 2498–2500
4. Mckenzie, D., Bartz, J., Mirwald, J., Olander, D., Marsh, R., and Aiken, J. (1998) *J. Biol. Chem.* **273,** 25545–25547
5. Culotta, V. C., Komp, L. W. J., Strain, J., Casareno, R. L. B., Krems, B., and Gitlin, J. D. (1997) *J. Biol. Chem.* **272,** 23469–23472
6. Roche, E., and Romero-Alvira, D. (1993) *Med. Hypotheses* **40,** 342–350
7. Shinobu, L. A., and Beal, M. F. (1997) in *Metals in Oxidative Damage in Neurological Disorders* (Conner, J. R., ed) Plenum, New York
8. Bush, A. (2003) *Trends Neurosci.* **26,** 207–214
9. Bush, A., Pettingell, W. H., Multhaup, G., Paradis, M., Vonsattel, J., Gusella, J. F., Beyreuther, K., Masters, C. L., and Tanzi, R. E. (1994) *Science* **265,** 1464–1467
10. Miura, T., Suzuki K., Kohata, N., and Takeuchi, H. (2000) *Biochemistry* **39,** 7024–7031
11. Ling, Y., Morgan, K., and Kalsheker, N. (2003) *Int. J. Biochem. Cell Biol.* **35,** 1505–1535
12. Kontush, A., Berndt, C., Weber, W., Akopian, V., Arlt, S., Schippling, S., and Beisiegel, U. (2001) *Free Rad. Biol. Med.* **30,** 119–128
13. Curtain, C., Ali, F., Volitakis, I., Cherny, R. A., Norton, R. S. Beyreuther, K., Barrow, C. J., Masters, C. L., and Bush, A. (2001) *J. Biol. Chem.* **276,** 20466–20473
14. Evin, G., and Weidemann, A. (2002) *Peptides* **23,** 1285–1297
15. Evin, G., Zhu, A., Holsinger, D., Masters, C. L., and Li, Q. (2003) *J. Neurosci. Res.* **74,** 386–392

16. Schőneich, C., Pogocki, D., Hug, G. L., and Bobrowski, K. (2003) *J. Am. Chem. Soc.* **125,** 13700–13713
17. Srivatsan, S. G., Nigam, P., Rao, M. S., and Verma, S. (2001) *Applied Catal. A* **209,** 327–334
18. Jang, J. H., and Surh, Y. J. (2002) *Ann. N. Y. Acad. Sci.* **973,** 228–236
19. Walter, M. F., Mason, P. E., and Mason, R. P. (1997) *Biochem. Biophys. Res. Commun.* **233,** 760–764
20. Lonrot, K., Metsa, K. T., Molnar, G., Ahonen, J. P., Latvala, M., Peltola, J., Pietila, T., and Alho, H. (1996) *Free Rad. Med. Biol.* **21,** 211–217
21. Nunomura, A., Perry, G., Zhang, J., Montine, T., Takeda, A., Chiba, S., and Smith, M. A. (1999) *J. Anti-Aging Med.* **2,** 227–230
22. Burrows, C. J., Lepentsiotis, V., Domagala, J., Grgic, I., van Eldik, R., and Muller, J. G. (1999) *Inorg. Chem.* **38,** 3500–3505
23. Aruoma, O. I., Halliwell, B., Gajewski, E., and Dizdaroglu, M. (1991) *Biochem. J.* **273,** 601–604
24. Sagripanti, J., and Kraemer, K. H. (1989) *J. Biol. Chem.* **264,** 1729–1734
25. Chiu, S.-m., Xue, L.-y., Friedman, L. R., and Oleinick, N. L. (1995) *Biochemistry* **34,** 2653–2661
26. Yamamoto, K., and Kawanishi, S. (1991) *J. Biol. Chem.* **266,** 1509–1515
27. Yamamoto, K., and Kawanishi, S (1989) *J. Biol. Chem.* **264,** 15435–15440
28. Kitajima, N., Koda, T., Iwata, Y., and Morooka, Y. (1990) *J. Am. Chem. Soc.* **112,** 8833–8839
29. Lewis, E. A., and Tolman, W. B. (2004) *Chem. Rev.* **104,** 1047–1076
30. Tolman, W. B. (1997) *Acc. Chem. Res.* **30,** 227–237
31. Stanulla, M., Wang, J., Chervinsky, D. S., Thandla, S., and Aplan, P. D. (1997) *Mol. Cell. Biol.* **17,** 4070–4079
32. Ehrenfeld, G. M., Rodriguez, L. O., and Hecht, S. M. (1985) *Biochemistry* **24,** 81–92
33. Zou, K., Gong., J. S., Yanagisawa, K., and Michikawa, M. (2002) *J. Neurosci.* **22,** 4833–4841
34. Kontush, A. (2001) *Free Radic. Med. Biol.* **31,** 1120–1131
35. Sigman, D. S., Mazumder, A., and Perrin, D. (1993) *Chem. Rev.* **93,** 2295–2316
36. Rao, P. S., Luber, J. M., Milinowicz, J., Lalezari, P., and Mueller, H. S. (1988) *Biochem. Biophys. Res. Commun.* **150,** 39–44
37. Bertini, I., Lippard, S. J., Gray, H. B., and Valentine, J. S. (eds) (1994) *Bioinorganic Chemistry*, Chap. 4 and 5, University Science Books, Sausalito, CA
38. Gerdemann, C., Eicken, C., and Krebs, B. (2002) *Acc. Chem. Res.* **35,** 183–191
39. Blackburn, N. J., Rhames, F. C., Ralle, M., and Jaron, S. (2000) *J. Biol. Inorg. Chem.* **5,** 341–353
40. Que, Jr., L., and Tolman, W. B. (2002) *Angew. Chem.* **41,** 1114–1137
41. Seo, S. Y., Sharma, V. K., and Sharma, N. (2003) *J. Agric. Food Chem.* **51,** 2837–2853
42. Chen, P., and Solomon, E. I. (2004**)** *J. Am. Chem. Soc.* **15,** 4991–5000
43. Yamazaki, S., and Itoh, S. (2003) *J. Am. Chem. Soc.* **125,** 13034–13035
44. Humphreys, K. J., Johnson, A. E., Karlin, K. D., and Rokita, S. E. (2002) *J. Biol. Inorg. Chem.* **7,** 835–842
45. Opazo, C., Huang, X., Cherny, R. A., Moir, R. D., Roher, A. E., White, A. R., Cappai, R., Masters, C. L., Tanzi, R. E., Inestrosa, N. C., and Bush, A. I. (2002) *J. Biol. Chem.* **277,** 40302–40308
46. Mahadevan, V., Henson, M. J., Solomon, E. I., and Stack, T. D. P. (2000) *J. Am. Chem. Soc.* **122,** 10249–10250
47. Bagchi, D., Garg, A., Krohn, R. L., Bagchi, M., Tran, M. X., and Stohs, S. J. (1997) *Res. Commun. Mol. Pathol. Pharmacol.* **95,** 179–189
48. Leskovac, V. (2002) *Comprehensive Enzyme Kinetics*, Kluwer/Plenum, Boston, MA
49. Florini, J. R., and Vestling, C. S. (1957) *Biochim. Biophys. Acta.* **25,** 575–578
50. Syme, C. D., Nadal, R. C., Rigby, S. E. J., and Viles, J. H. (2004) *J. Biol. Chem.* **279,** 18169–18177
51. Atwood, C. S., Scarpa, R. C., Huang, X., Moir, R. D. Jones, W. D. Fairlie, D. P., Tanzi, R. E., and Bush, A. I. (2000) *J. Neurochem.* **75,** 1219–1233
52. Hegg, E. L., Mortimore, S. H., Cheung, C. L., Huyett, J. E., Powell, D. R., and Burstyn, J. N. (1999) *Inorg. Chem.* **38,** 2961–2968
53. Garzon-Rodriguez, W., Yatsimirsky, A. K., and Glabe, C. G. (1999) *Bioorg. Med. Chem. Lett.* **9,** 2243–2248
54. Huang, X., Atwood, C. S., Moir, R. D., Hartshorn, M. A., Tanzi, R. E., and Bush, A. I. (2004) *J. Biol. Inorg. Chem.*, **9,** 954–960
55. Kowalik-Jankowska, T., Ruta, M., Wiśniewska, K., and Łankiewicz, L. (2003) *J. Inorg. Biochem.* **95,** 270–282
56. Lever, A. B. P. (1986) *Inorganic Electronic Spectroscopy*, 2nd Ed., pp. 554–567, Elsevier, New York
57. Cotton, F. A., and Wilkinson, G. (1988) *Advanced Inorganic Chemistry,* 5th Ed., p. 865, Wiley, New York, NY
58. Bertini, I., and Luchinat, C. (1984) *Adv. Inorg. Biochem.* **6,** 71–111
59. Ming, L.-J. (2000) in *Physical Methods in Bioinorganic Chemistry, Spectroscopy and Magnetism* (Que, L., Jr., ed) Chapter 8, University Science Books, Sausalito, CA
60. Burger, A. R., Lippard, S. J., Pantoliano, M. W., and Valentine, J. S. (1980) *Biochemistry* **19,** 4139–4143
61. Miura, T., Suzuki K., and Takeuchi, H. (2001) *J. Mol. Struct.* **598,** 79–84
62. Park, H. I., and Ming, L. J. (1998) *J. Inorg. Biochem.* **72,** 57–62